Accepted Manuscript

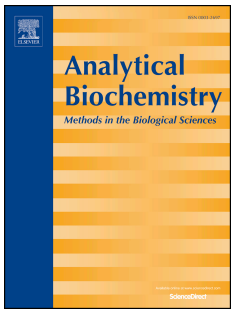

An impedimetric micro-immunosensing assay to detect Alzheimer's disease biomarker: Aβ40

Norazreen Zakaria, Muhammad Zaki Ramli, Kalavathy Ramasamy, Lim Siong Meng, Chan Yean Yean, Kirnpal Kaur Banga Singh, Zainiharyati Mohd Zain, Kim-Fatt Low

PII: S0003-2697(18)30273-2

DOI: 10.1016/j.ab.2018.05.031

Reference: YABIO 13037

To appear in: *Analytical Biochemistry*

Received Date: 14 March 2018

Revised Date: 23 May 2018

Accepted Date: 30 May 2018

Please cite this article as: N. Zakaria, M.Z. Ramli, K. Ramasamy, L.S. Meng, C.Y. Yean, K.K. Banga Singh, Z.M. Zain, K.-F. Low, An impedimetric micro-immunosensing assay to detect Alzheimer's disease biomarker: Aβ40, *Analytical Biochemistry* (2018), doi: 10.1016/j.ab.2018.05.031.

An impedimetric micro-immunosensing assay to detect Alzheimer's disease biomarker: Aβ40

Norazreen Zakaria [a], Muhammad Zaki Ramli [b], Kalavathy Ramasamy [b], Lim Siong Meng [b], Chan Yean Yean [c], Kirnpal Kaur Banga Singh [c], Zainiharyati Mohd Zain [a,*], Kim-Fatt Low [a, d, *]

[a] *Electrochemical Material and Sensors (EmaS) Group, Faculty of Applied Sciences, Universiti Teknologi MARA, 40450 Shah Alam, Selangor, Malaysia*

[b] *Collaborative Drug Discovery Research (CDDR) Group, Faculty of Pharmacy, Universiti Teknologi MARA, Puncak Alam Campus, 43600 Bandar Puncak Alam, Selangor, Malaysia*

[c] *Department of Medical Microbiology and Parasitology, School of Medical Sciences, Universiti Sains Malaysia, 16150 Kubang Kerian, Kelantan, Malaysia*

[d] *Faculty of Applied Sciences, Universiti Teknologi MARA, Tapah Campus, 35400 Tapah Road, Perak, Malaysia*

* Corresponding authors.

E-mail addresses: zainihar@salam.uitm.edu.my (Z. M. Zain), lowkimfatt@hotmail.my; lowkimfatt@perak.uitm.edu.my (K.-F. Low).

ABSTRACT

A miniaturized biosensing platform, based on monoclonal amyloid-beta antibodies (*m*$A\beta_{ab}$) that were immobilized on a disc-shaped platinum/iridium (Pt/Ir) microelectrode surface coupled with an impedimetric signal transducer, was developed for the label-free and sensitive detection of amyloid-beta peptide fragment 1−40 (Aβ40); a reliable biomarker for early diagnosis of Alzheimer's disease (AD). A Pt/Ir microelectrode was electropolymerized with poly(ortho-phenylenediamine), a conducting free amine-containing aromatic polymer; followed by crosslinking with glutaraldehyde for subsequent coupling of *m*$A\beta_{ab}$ on the microelectrode surface. This modification strategy efficiently improved the impedimetric detection performance of Aβ40 in terms of charge transfer resistance (~400-fold difference) and normalized impedance magnitude percentage change (~40% increase) compared with a passive adsorption-based immobilization method. The sensitivity of the micro-immunosensing assay was found to be 1056 kΩ/(pg/mL)/cm^2 and the limit of detection was found to be 4.81 pg/mL with a dynamic range of 1−10^4 pg/mL (R^2=0.9932). The overall precision of the assay, as measured by relative standard deviation, ranged from 0.84−5.15%, demonstrating its reliability and accuracy; while in respect to assay durability and stability, the immobilized *m*$A\beta_{ab}$ were able to maintain 80% of their binding activity to Aβ40 after incubation for 48 h at ambient temperature (25 °C). To validate the practical applicability, the assay was tested using brain tissue lysates prepared from AD-induced rats. Results indicate that the proposed impedimetric micro-immunosensing platform is highly versatile and adaptable for the quantitative detection of other disease-related biomarkers.

Keywords:

Conducting polymer; Crosslinker; Covalent immobilization; Impedimetric biosensor; Microelectrode; Amyloid-beta

1. Introduction

Alzheimer's disease (AD) is characterized behaviorally by progressive memory and cognitive decline and physiologically by the presence of two established pathophysiological hallmarks in the brain: extracellular accumulations of amyloid-beta peptide (Aβ) and intracellular neurofibrillar tangles of hyper-phosphorylated tau protein [1, 2]. Aβ is generated by the sequential cleavage of amyloid precursor protein (APP) resulting in the production of variable lengths of Aβ, predominantly of 40 and 42 amino acids (Aβ40 and Aβ42, respectively) [3-5]. In healthy individuals, Aβ40 is the most abundant form of Aβ present in human brain; however, Aβ40 can undergo an aggregation process resulting in the presence of toxic insoluble plaques that are the hallmarks of AD [6-8].

Currently, enzyme-linked immunoassays (ELISA) are the most prevalent detection platforms for identifying trace amounts of Aβ. However, although reliable ELISA are time consuming and their dependence on labeled bioreagents may lead to decreased sensitivity due to reduced biomolecular activities [9-11]. In this context, a rapid, label-free analytical method would offer an attractive option for overcoming these problems associated with ELISA. Up to date, a few label-free analytical platforms including surface-enhanced Raman spectroscopy (SERS) [12], interferometric reflectance imaging sensor (IRIS) [13], localized surface plasmon resonance (LSPR) [14], piezoelectric-driven microslit cantilever [15], matrix assisted laser desorption ionization mass spectrometry (MALDI-MS) [16], total internal reflection ellipsometry (TIRE) [17], and electrospray ionization mass spectrometry (ESI-MS) [18] have gained scientific attention for Aβ detection. Regrettably, most of these platforms are often costly, require sophisticated laboratory instruments and well-trained personnel for operation.

An impedimetric immunosensing assay, based on the integration of specific surface antibodies as a bioreceptor and an electrochemical impedance spectroscopy (EIS) signal transducer presents a promising alternative for Aβ detection. This type of assay has inherent specificity and selectivity as it provides antigen–antibody biospecific interaction on electrode surfaces, and at the same time, offers the advantages of EIS-based biosensing technology, including: label-free detection capabilities, cost-effectiveness, high sensitivity, simple operation, and easy miniaturization via microfabrication [19]. The use of EIS techniques for immunosensing application is based on the premise that an affinity interaction between an antigenic bioreceptor and its targets/analytes causes a change in the charge transfer kinetics occurring across an electrode–electrolyte interface [20]. Thus, by having sensitive ability to detect this minute change in the interfacial impedance the need for introducing electroactive labels/tags to the antigen–antibody biorecognition events could be eliminated during EIS measurements. In addition, in contrast to other electroanalytical techniques such as chronoamperometry (CA), cyclic voltammetry (CV), differential pulse voltammetry (DPV) or square wave voltammetry (SWV) that are all reliant on large, abrupt excitation signals for measurement, EIS is a non-destructive technique of electroanalysis as it applies only very small-amplitude excitation signals without significantly disturbing the properties being measured, leading to a stable and reliable immunosensing platform [21, 22].

A critical aspect of immunosensing assay development is the antibody immobilization strategy: A stable antigen–antibody immobilization on detection surfaces with a complete retention of their biological recognition properties is crucial for successful construction of an immunosensing assay. Previously, we reported an immunosensing assay based on passive physical adsorption of antibodies on a platinum/iridium (Pt/Ir) microelectrode surface for the

impedimetric detection of a disease biomarker [23]. This reported assay enabled label-free, rapid, and highly biospecific detection of the biomarker; however, it exhibited less sensitivity than other reported studies [24, 25] and further improvement in surface chemistry modification was needed to enhance assay sensitivity. Here, an improved antibody immobilization strategy (Fig. 1) in which the Pt/Ir microelectrode surface was modified with poly(ortho-phenylenediamine) (PoPD) via electropolymerization, followed by covalent coupling of monoclonal amyloid-beta antibodies (*m*$A\beta_{ab}$) through crosslinking with glutaraldehyde (GA) on the microelectrode surface is described. GA is a bifunctional compound that has been mainly used in chemical modifications of proteins and polymers; and in this study, GA covalently linked to the amine groups of lysine or hydroxylysine in the *m*$A\beta_{ab}$, creating a stable 'click compound' on the microelectrode surface [26]. The covalently immobilized *m*$A\beta_{ab}$ was then used to bind the detection target, Aβ40. Quantitative electrochemical detection of the Aβ40−*m*$A\beta_{ab}$ binding on the GA–PoPD-modified micro-immunosensing surface was achieved using an impedance technique. Results indicated that the GA crosslinking-covalent coupling strategy was able to improve the immobilization efficiency of *m*$A\beta_{ab}$ on the PoPD-modified Pt/Ir microelectrode surface and significantly increased the sensitivity by lowering the detection limit of the assay against Aβ40.

2. Material and methods

2.1. Chemicals

Ortho-phenylenediamine (oPD), sodium chloride (NaCl), sodium phosphate monobasic (NaH_2PO_4), GA, Aβ40 (1.0 mg), and mouse *m*$A\beta_{ab}$ (1.5 mg/mL) were purchased from Sigma-Aldrich (Missouri, USA). Sodium hydroxide (NaOH) was supplied from Merck (Darmstadt,

Germany). All chemicals were used without further purification. The buffer solution used was phosphate-buffered saline (PBS; pH 7.4, containing 0.1 M NaH_2PO_4, 3 M NaCl and 0.9 M NaOH). All aqueous solutions were made in deionized water (*de*H_2O) obtained from an Arium® pro purification system (Sartorius, Goettingen, Germany).

2.2. Apparatus

All electroanalytical measurements were performed using an Autolab PG STAT302 potentiostat/galvanostat (Eco Chemie, Utrecht, The Netherlands) controlled by Nova 1.11 software. A three-electrode electrochemical cell consisting of a disc-shaped Pt/Ir microelectrode as a working electrode, a Pt rod counter electrode, and an Ag/AgCl reference electrode, was employed for impedimetric measurements using the setup depicted in Fig. S1 in the supplementary data section. All the electrodes were firmly held in a fixed position by a customized Teflon cell top with the detection ends immersed 2 cm into a cell vial (dimension: 25.6 mm inner diameter × 50 mm height) containing 20 mL of PBS electrolyte solution, and the other ends of the electrodes were connected to the potentiostat instrument through alligator clips. The length of the three electrodes immersed in the electrolyte was kept unchanged (2 cm) in all the experiments in order to maintain a constant electrode surface area for measuring electrode–electrolyte interface impedance. The surface morphologies of the micro-immunosensing surface were analysed using a Supra™ 40VP field emission scanning electron microscopy (FESEM) system (Carl Zeiss, Oberkochen, Germany).

2.3. Fabrication of a disc-shaped *Pt/Ir microelectrode*

A Teflon-coated Pt/Ir wire (inner diameter: 50 μm) (Advent Material, Odford, UK) was cut to a length of 3 cm using a scalpel. Next, the outer Teflon coating layer at one end of the Pt/Ir wire was stripped to expose 0.5 cm inner bare Pt/Ir wire after which the exposed end was soldered with a gold connector to facilitate the connection as a working electrode to the potentiostat instrument. The disc-shaped microelectrode surface was prepared by making a transverse path that cut across the other end of the Teflon-coated Pt/Ir wire to produce a smooth tip end detection surface (Fig. S2 in the supplementary data section).

2.4. Biofunctionalization of the Pt/Ir microelectrode surface

The Pt/Ir microelectrode surface was modified with PoPD via electropolymerization of 300 mM oPD in PBS using a chronoamperometry technique at +0.70 V for 30 min followed by rinsing with *de*H_2O to remove any unbound or unreacted oPD monomer. The resulting PoPD-modified Pt/Ir microelectrode was then biofunctionalized with *m*$A\beta_{ab}$ via cross-linkage with GA—the two functional aldehyde groups of GA easily form stable covalent amide bonds with the amine groups of the PoPD layer on the Pt/Ir microelectrode surface and those of the *m*$A\beta_{ab}$. Firstly, the PoPD-modified Pt/Ir microelectrode was incubated in 3 μL of 25% (v/v) GA in PBS for 30 min, rinsed with *de*H_2O to remove residual GA, and left to dry at ambient temperature for approximately 5 min. Next, the microelectrode was incubated in 3 μL of 10^5 pg/mL *m*$A\beta_{ab}$ in PBS for 30 min at ambient temperature and rinsed again with *de*H_2O. The biofunctionalized microelectrode was either immediately used for impedimetric measurement or kept at 4 °C in PBS until further use.

2.5 Electrochemical impedance spectroscopy (EIS)

A three-electrode electrochemical cell was set up as described in Section 2.2. The *m*$A\beta_{ab}$–GA–PoPD-modified Pt/Ir microelectrode was used as a working electrode and immersed in 20 mL of PBS containing different concentrations of Aβ40. The electrochemical cell was incubated for 20 min at ambient temperature to allow binding to occur. Impedimetric-quantitative analyses of the Aβ40-*m*$A\beta_{ab}$ immune complexes formed on the micro-immunosensing surface were then performed using EIS at frequencies ranging from 10^{-1}–10^{5} Hz with an excitation amplitude of 10 mV. The resulting impedance signals were displayed in Nyquist format by plotting the real impedance component (Z') against the imaginary impedance component (Z"). In the absence of a redox probe (e.g. Fe^{2+}/Fe^{3+}), the resulting impedance signal was caused by Aβ40 that adhered to the electrode surface [27]. The diameter of the semicircle extrapolated in the Nyquist plots represented the charge transfer resistance (R_{ct}) that provided information on the charge transfer kinetics at the electrode–electrolyte interface. The R_{ct} was determined by fitting the Nyquist plots with a modified equivalent circuit model.

2.6 Animal grouping and brain tissue lysate preparation

Sprague-Dawley rats (adult male; 250−300 g; gifts from the Collaborative Drug Discovery Research Group, Faculty of Pharmacy, Universiti Teknologi MARA (UiTM), Puncak Alam Campus, Malaysia) were divided into five different experimental treatment groups (Table 1). All animals received housing and food and water, and all subsequent experiments were in accordance with the ethical guidelines of UiTM Committee on Animal Research and Ethics (Animal Ethics Clerance Reference No: 600-FF PT.5/2).

Brain tissue lysates were prepared as previously described [28], with minor modifications. Briefly, animals were sacrificed by cervical dislocation and their brains were rapidly dissected out. Brains were then homogenized using a glass homogenizer (WiseStir®, Wertheim, Germany) in ice-cold PBS and the resultant lysate was centrifuged at 2000 ×g, for 10 min at 4 °C. Finally, the supernatant was collected and stored at −80 °C until further use.

2.6.1 Impedimetric micro-immunosensing of Aβ40 in brain tissue lysates

The *m*$A\beta_{ab}$–GA–PoPD-modified Pt/Ir microelectrode was immersed in 5 μL of brain tissue lysate mixed with 20 mL PBS and impedimetric-quantitative analyses of the resultant Aβ40−*m*$A\beta_{ab}$ immune complexes were performed using EIS. The changes of impedance were observed before (control) and after the addition of samples.

2.6.2 ELISA

The presence of Aβ40 in brain tissue lysates was verified using the High Sensitivity Aβ40 ELISA kit (Milipore, Missouri, USA) according to the manufacturer's instructions. Generally, the entire ELISA procedures for detecting Aβ40 required about two days using a 50 μL sample volume and with a detection range of 16–500 pg/mL. The absorbance was measured at 450 nm and 590 nm, respectively, using a microplate reader (TECAN, Männedorf, Switzerland).

3. Results and Discussion

3.1 Equivalent circuit model for impedimetric micro-immunosensing

Impedimetric micro-immunosensing is based on the principle that the formation of antigen–antibody immune complexes on the microelectrode will result in impedance changes at the

electrode–electrolyte interface. In this study, the formation of Aβ40–*m*$A\beta_{ab}$ immune complexes was observed to affect the impedance signal at the interfaces between the Pt/Ir microelectrode and the PBS electrolyte solution; while Nyquist plots were used to investigate this particular impedance changes. These plots were then fitted with an equivalent circuit model (Fig. 2) consisting of the following parameters: resistance of the solution (R_s); Warburg impedance (Z_w); three elements of the R_{ct}: protein adsorption resistance (R_{ctads}), protein film resistance (R_{ctfilm}), and pore resistance (R_{ctpore}); and the corresponding constant phase element (CPE): CPE_{ads}, CPE_{film}, and CPE_{pore}. The equivalent circuit was made up of three circuit components: at the high frequency the impedance signal was due to the R_{ctpore}/CPE_{pore} on Pt/Ir microelectrode surface; at the middle frequency the impedance signal was due to the R_{ctfilm}/CPE_{film}; and at the lower frequency it was due to the R_{ctads}/CPE_{ads}.

The binding of Aβ40 to the micro-immunosensing surface was described as the formation of a barrier to the current flow with the R_{ctads}, which represented the partial charge transfer from the strongly bound Aβ40 at the microelectrode surface; and also the CPE_{ads} which accounted for the adsorption of electroactive species and charging of the double layer [29]. The association binding constant (k_a) between Aβ40 and *m*$A\beta_{ab}$ immobilized on the microelectrode surface was determined to be k_a = 0.933 pg/mL (discussed in detail in the supplementary data section), indicating that there were less free spaces on the microelectrode surface for other electroactive species to be discharged, and as a result, the electrochemical behavior was deduced to be a combination of R_{ctads}/CPE_{ads} at low frequency [30]. The R_{ctads} value was chosen for quantitative impedimetric detection of Aβ40 as it was empirically found to be strongly correlated to the modification and biorecognition events that occurred on the microelectrode surface (data not shown).

3.2 Characterization of biofunctionalized Pt/Ir microelectrode

Following the electropolymerization with a PoPD layer, the Pt/Ir was biofunctionalized with *m*$A\beta_{ab}$ via a GA crosslinking-covalent coupling strategy to enhance Aβ40 detection. The reaction mechanisms involved in the biofunctionalization of the Pt/Ir microelectrode surface are depicted in Fig. 3.

3.2.1 Surface characterization using FESEM

The surface morphologies of the Pt/Ir microelectrode before and after biofunctionalization were characterized by FESEM, as shown in Fig. 4A. The bare Pt/Ir microelectrode showed a smooth metallic surface (Fig. 4Ai) and transformed to a compact layer of wrinkled, flake-like structures following the electropolymerization of the PoPD on the microelectrode surface (Fig. 4Aii). After crosslinking with GA, the *m*$A\beta_{ab}$ was covalently immobilized on the microelectrode surface, resulting in a dense, porous, and inhomogeneous surface appearance (Fig. 4Aiii). The immuno-capturing of Aβ40 on the *m*$A\beta_{ab}$–GA–PoPD-modified Pt/Ir microelectrode resulted in scattered, granular-like structures (Fig. 4Aiv), which might be attributed to the formation of Aβ40 aggregates and amyloid plaques on the microelectrode surface [31].

3.2.2 Electrochemical characterization using EIS

EIS was performed on the Pt/Ir microelectrode following each biofunctionalization step, which included PoPD electropolymerization, GA crosslinking, *m*$A\beta_{ab}$ immobilization, and Aβ40 immuno-capturing, using PBS as the electrolyte solution. The value of the polarization potential was fixed at −0.2 V, where at this applied potential, the formation of Aβ40–*m*$A\beta_{ab}$ immune

complexes on the microelectrode surface exhibited impedance responses, resulting in the appearance of single depressed semicircles in the Nyquist plots.

Fig. 4B shows the Nyquist plots of different modification layers carried out on the Pt/Ir microelectrode surface. There was a change in the semicircle diameter (representing R_{ct}) after each modification step on the Pt/Ir microelectrode surface. The Nyquist plot that included both the semicircle and a linear region could only found on the bare Pt/Ir microelectrode (control surface) and PoPD-modified Pt/Ir microelectrode. The semicircle diameter at higher frequencies corresponded to R_{ct}, which controlled the charge transfer kinetics at the electrode–electrolyte interface; while at lower frequencies, the linear region was associated with the typical trend of a mass diffusion-limited electron-transfer process [32]. The R_{ct} for the PoPD-modified Pt/Ir microelectrode (68.8 ± 3.9 kΩ; n = 3; Fig. 4B, x-line) was significantly smaller than that of the bare Pt/Ir microelectrode (439 ± 0.18 kΩ; n = 3; Fig. 4B, inset), revealing that PoPD increased the electroactive surface area of the microelectrode. This resulted in easier electron transfer from the PBS electrolyte solution to the microelectrode, due to increased diffusion of small electrolyte species onto the surface of the charged PoPD layer [33]. Interestingly, R_{ct} decreased further to 16.6 ± 2.8 (n =3; Fig. 4B, □-line), and 10.5 ± 6.8 (n =3; Fig. 4B, Δ-line) after surface activation with GA crosslinkers and subsequent covalent immobilization of *m*$A\beta_{ab}$ onto the PoPD-modified Pt/Ir microelectrode, respectively; revealing that GA effectively immobilized and crosslinked *m*$A\beta_{ab}$. It can be assumed that there were favourable molecular arrangements of immobilized *m*$A\beta_{ab}$ that presented better orientation onto the surface of GA–PoPD-modified Pt/Ir microelectrode [34]. Therefore, the *m*$A\beta_{ab}$–GA–PoPD-modified Pt/Ir microelectrode allowed easier electron transfer due to increased active sites for electrical contact between the microelectrode and the electrolyte species in PBS solution. The R_{ct} for the Aβ40 bound *m*$A\beta_{ab}$–

GA–PoPD-modified Pt/Ir microelectrode increased to 13.9 ± 3.6 (n =3; Fig. 4B, ◊-line), revealing that the formation of Aβ40−*m*$A\beta_{ab}$ immune complexes exerted surface blocking effects resulting in a reduction of electron transfer to the Pt/Ir microelectrode.

3.3. Impedance responses on passive adsorption and covalent immobilization of m$A\beta_{ab}$

The proposed micro-immunosensing assay is an affinity-based assay that uses *m*$A\beta_{ab}$ to specifically bind to target Aβ40, where the binding affinity of Aβ40–*m*$A\beta_{ab}$ interaction defines the analytical performance of the assay. The immobilization of *m*$A\beta_{ab}$ is a crucial step in the development of the micro-immunosensing assay. In this study, two *m*$A\beta_{ab}$ immobilization strategies were examined to determine their electrochemical impedance response towards Aβ40. The *m*$A\beta_{ab}$ immobilization mechanisms included: (i) covalent binding through GA crosslinking to the PoPD-modified Pt/Ir microelectrode surface, and (ii) passive adsorption onto the PoPD-modified Pt/Ir microelectrode surface.

Nyquist plots showed substantial differences in depressed semicircles obtained from the micro-immunosensing assay based on the covalent immobilization strategy compared with the passive adsorption strategy (Fig. S3A in the supplementary data section). The R_{ct} values were extracted from a modified equivalent circuit as discussed in Section 3.1. Here, the R_{ct} for the micro-immunosensing assay using the GA crosslinking reaction showed a higher value (13.9 ± 3.6 kΩ; n = 3) compared with the passive adsorption strategy (0.032 ± 0.001 kΩ; n = 3). This 400-fold increase in the R_{ct} value from the GA-modified Pt/Ir microelectrode could be attributed to free terminal amine groups in PoPD reacting with carbonyl groups in GA resulting in production of amine-reactive aldehyde ends that function as binding sites for stable immobilization of *m*$A\beta_{ab}$ and also maintain the antibodies in their native conformation,

consequently increasing *m*Aβ$_{ab}$ binding capacity for Aβ40 [26]. Meanwhile, the lower R_{ct} values obtained from the non-GA-modified microelectrode may be attributed to inefficient immobilization of *m*Aβ$_{ab,}$ thereby reducing the capture efficiency of Aβ40. In addition, comparisons between the GA-modified microelectrode and adsorbent microelectrode were also determined for the variation of the normalized impedance magnitude percentage change (ΔZ) in selected frequencies ranging from 100 kHz to 1 kHz (Fig. S3B in the supplementary data section) based on following equation (1) [35]:

$$\Delta Z = \frac{Z(\text{with GA crosslinking})-Z\ (\text{without GA crosslinking})}{Z\ (\text{with GA crosslinking})} \times 100 \qquad (1)$$

The calculated ΔZ showed that the micro-immunosensing assay with GA crosslinking was ~40% higher (at ~10.5 kHz) than the passive adsorption counterpart, revealing that the former was able to enhance the immobilization of *m*Aβ$_{ab}$ on the PoPD-modified Pt/Ir microelectrode surface and significantly improved the affinity binding for Aβ40.

3.4 Optimization of assay variables

The variables affecting the impedimetric micro-immunosensing assay performance, the GA concentration, *m*Aβ$_{ab}$ concentration, and incubation time of antigen–antibody binding, were sequentially optimized by detection against 10^7 pg/mL of Aβ40.

In this study, *m*Aβ$_{ab}$ were covalently immobilized onto Pt/Ir microelectrode surface previously modified with a GA-crosslinked layer of PoPD. GA is a bifunctional linker with two aldehyde groups in both ends of its molecular structure that could form stable covalent amide bonds with the amine groups of the PoPD layer on the Pt/Ir microelectrode surface and those of

the *m*$A\beta_{ab}$. An optimal concentrations of GA and *m*$A\beta_{ab}$ are necessitated to form a stable monolayer of *m*$A\beta_{ab}$ on the Pt/Ir microelectrode surface for capturing more Aβ40. The effects of increasing GA concentration (0–55% (v/v)) and *m*$A\beta_{ab}$ concentration (0–10^6 pg/mL) are shown in Fig. S4A and S4B in the supplementary data section, respectively. Taking into account the intensity of R_{ct} and repeatability in terms of standard deviation, the GA and *m*$A\beta_{ab}$ concentrations were found to be optimal on 25% (v/v) and 10^5 pg/mL, respectively.

The incubation time required for the antigen–antibody binding is also the important variable that would affect the detection range of Aβ40. Fig. S4C in the supplementary data section depicts the effect of increasing incubation time (5–60 min) on impedimetric responses of the micro-immunosensing assay. As can be seen, R_{ct} exhibited the continuous rise during 20 min incubation, indicating that more and more Aβ40 were captured by the micro-immunosensing assay with the time accumulation. However, the R_{ct} reached a plateau after 20 min, suggesting that the amount of Aβ40 captured on the micro-immunosensing surface was saturated. Hence, the optimal incubation time for the immunological binding between *m*$A\beta_{ab}$ and Aβ40 was 20 min.

3.5 Analytical performance of the impedimetric micro-immunosensing assay

The analytical sensitivity of the detection platform was evaluated by testing against a known amount of serially diluted Aβ40 (1–10^7 pg/mL). Fig. 5A displays the obtained Nyquist plots. Data show that the R_{ct} increased with increasing concentrations of Aβ40; observed directly from the diameter of the semicircle in the Nyquist plots. In the presence of increased Aβ40 concentrations, the formation of Aβ40−*m*$A\beta_{ab}$ immune complexes likely lead to blockage of any remaining free spaces on the micro-immunosensing surface and thus resulted in a larger diameter of the corresponding semicircle in the respective Nyquist plot [9]. The calibration curve showed

a good linear relationship between the $1/R_{ct}$ and the Aβ40 concentration in the range of $\log_{10}$ (1–10^4 pg/mL) with a coefficient of determination (R^2) of 0.9932, indicating that the response was the direct result of Aβ40 binding to the *m*$A\beta_{ab}$–GA–PoPD-modified Pt/Ir microelectrode through antigen–antibody biospecific interaction. All experiments were performed in triplicate, and the relative standard deviation (RSD) values were 1.23−5.12%. The limit of detection (LoD) was calculated based on standard deviation of the blank sample and slope of calibration curve according to the following equation (2):

$$\text{LoD} = \frac{3 \times \text{standard deviation}}{\text{Slope}} \qquad (2)$$

The LoD of the impedimetric micro-immunosensing assay was determined to be 4.81 pg/mL of Aβ40, which was the lowest among the recently reported label-free electrochemical immunosensing platforms as listed in Table 2. Out of these six immunosensing assays [23, 36-40], only two [36, 37] have a LoD in the same range as the one achieved in this study but showing fairly narrow linear dynamic range of detection and/or involving much more complex detection scheme.

The sensitivity of the impedimetric micro-immunosensing assay was also calculated based on following equation (3):

$$\text{Sensitivity} = \frac{\text{Slope of calibration plot}}{\text{Active surface area, } A\ (\text{cm}^2)} \qquad (3)$$

Where, '*A*' is the geometrical dimension of the Pt/Ir microelectrode and was calculated to be 1.96 x 10^{-5} cm^2. Based on this '*A*' value, the sensitivity was determined to be 1056

kΩ/(pg/mL)/cm^2 which was a 100-fold increase compared to our previously reported study based on passive adsorption strategy (10.20 kΩ/(pg/mL)/cm^2) [23].

We subsequently performed an analytical specificity study by incubating *m*Aβ_{ab}–GA–PoPD-modified Pt/Ir microelectrode with neurochemicals commonly found in cerebrospinal fluid, including ascorbic acid (AA), uric acid (UA), and 4-dihydroxylphenylacetic acid (DOPAC); all of which would have likely interfered with the detection of Aβ40 in brain lysate samples [41, 42]. Fig. 5B compares the obtained Nyquist plots before (control) and after the interactions with AA, UA, DOPAC, and Aβ40 at concentrations of 250 μM, 20 μM, 10 μM, and 4.81 pg/mL, respectively. It is noteworthy that the concentrations of the interference species being studied were far higher than the normal levels presented in human cerebrospinal fluid [43]. The absence of antigen–antibody interactions is clear, since the R_{ct} of AA, UA, and DOPAC were similar to the control and much lower than that of Aβ40. The RSD values of this study were 0.98−5.15%. These results indicated that the micro-immunosensing assay resisted interference well and demonstrated excellent specificity.

3.6 Repeatability, durability and stability.

Repeatability, stability, and durability are among the major concerns in all assay development. The repeatability of the impedimetric micro-immunosensing assay was investigated by detecting 4.81 pg/mL of Aβ40 for ten replicates on 10 different days. The corresponding R_{ct} was highly consistent (data not shown) with a low RSD value of 0.84% indicating excellent repeatability of the developed assay. In addition, we determined assay durability and stability by incubating a *m*Aβ_{ab}–GA–PoPD-modified Pt/Ir microelectrode in PBS solution for 48 h at ambient temperature (25 °C) prior to Aβ40 detection. After 48 h the microelectrode maintained 80% of its binding

capacity for Aβ40, indicating the covalently immobilized *m*$A\beta_{ab}$ was highly stable on the Pt/Ir microelectrode surface. This finding was significantly higher compared with the passive adsorption strategy that only maintained 3.2% after 48 h [23].

Overall, the proposed GA crosslinking-covalent coupling strategy significantly enhanced the repeatability, stability, and durability of *m*$A\beta_{ab}$ immobilized on the sensing surface; and therefore exhibit appropriate feature for analytical purposes.

3.7 Diagnostic evaluation with brain tissue lysate

The impedimetric micro-immunosensing assay was further evaluated using brain tissue lysate samples prepared from rodent models mimicking AD induced by injection of synthetic Aβ into the brain. It is worth noting that synthetic Aβ injection initiates neurotoxic effects including: the production of amyloidogenic APP fragments, which stimulate neurons to cleave Aβ into its two main forms: Aβ40 and Aβ42 [44]. Hence, the detection of Aβ40 in the brain tissue lysate was possible using the Aβ40-specific impedimetric micro-immunosensing assay.

Obtained results were validated against the responses measured with ELISA using the same brain tissue lysate samples. The corresponding R_{ct} values for the impedimetric micro-immunosensing assay and the absorbance values of ELISA were translated into Aβ40 concentrations using respective calibration plots. By comparing the developed impedimetric micro-immunosensing assay with a similar immunodiagnostic assay, the ELISA, the usefulness of the former as a diagnostic platform for AD was thus evaluated.

Fig. 6 compares the Aβ40 concentrations determined by the impedimetric micro-immunosensing assay and ELISA for brain tissue lysate samples prepared from different groups of rats (Table 1). Both assays showed similar diagnostic performance characteristics in which in

all the groups tested (WT, SH, AD+O, and AD+IB), there were lower concentrations of Aβ40 compared with the AD control group. The RSD values for the impedimetric micro-immunosensing assay and ELISA were 0.99−4.03% and 3.8−10.64%, respectively. Generally, the Aβ40 concentrations detected using the impedimetric micro-immunosensing assay were slightly lower than the ELISA. This variation was likely due to the difference in the Aβ40 standard used to establish calibration plots and the ability to immobilize larger amounts of antibodies on ELISA microplate surface [45]. Nevertheless, it is notable that the impedimetric micro-immunosensing assay presented a lower LoD (4.81 pg/mL) compared with the ELISA (≥16 pg/mL). These comparative studies showed that the impedimetric micro-immunosensing assay was able to achieve rapid, label-free detection of Aβ40; and therefore we believe this assay offers a promising alternative to the conventional ELISA method.

4. Conclusion

The detailed development of a highly sensitive biosensing assay for quantitative electrochemical detection of the AD biomarker, Aβ40, has been presented. We demonstrated GA crosslinking was able to improve the immobilization of $m\text{A}\beta_{ab}$ as a biorecognition element for Aβ40 on a PoPD-modified Pt/Ir microelectrode. Furthermore, the use of GA crosslinking-covalent coupling strategy was empirically shown to enhance assay performance in various aspects including: assay precision (RSD = 0.84−5.15%), stability (retaining 80% of assay activity after 48 h incubation time), and sensitivity (LoD = 4.81 pg/mL). Non faradaic EIS measurements were performed and the obtained R_{ct} changed linearly with Aβ40 concentrations within the range of $1–10^4$ pg/mL. The real diagnostic applicability of the impedimetric immunosensing assay was evaluated using brain tissue lysate samples and its diagnostic

performance was proven to be more effective than conventional ELISA in terms of assay simplicity, sample volume consumption, and lowest detection limit. In addition, the application of an electric field-driven strategy in this biosensing assay significantly reduced the time it took to quantify Aβ40 compared with ELISA— 1.5 h compared with 2 days. These results, along with the compact size of the microelectrode and the reagent-free analysis capability using impedance techniques, suggest that this biosensing assay are a powerful tool in the imminent future for in-vivo, real-time detection of Aβ40 in the human brain and may be a potential alternative for AD diagnosis.

Acknowledgements

This research was financially supported by Ministry of Education, Malaysia in the form of a FRGS grant (FRGS/1/2015/SG05/UITM/02/7). We would like also to acknowledge Faculty of Applied Sciences, Universiti Teknologi MARA Malaysia (UiTM) for providing infrastructural facilities during the research project.

References

[1] D. Brambilla, B. Le Droumaguet, J. Nicolas, S.H. Hashemi, L.P. Wu, S.M. Moghimi, et al., Nanotechnologies for Alzheimer's disease: diagnosis, therapy, and safety issues, Nanomedicine 7 (2011) 521–540.

[2] J. Pahnke, L.C. Walker, K. Scheffler, M. Krohn, Alzheimer's disease and blood-brain barrier function-Why have anti-β-amyloid therapies failed to prevent dementia progression?, Neurosci. Biobehav. Rev. 33 (2009) 1099–1108.

[3] M. Bartolini, M. Naldi, J. Fiori, F. Valle, F. Biscarini, D.V. Nicolau, et al., Kinetic characterization of amyloid-beta 1–42 aggregation with a multimethodological approach, Anal. Biochem. 414 (2011) 215–225.

[4] M.A. Findeis, The role of amyloid beta peptide 42 in Alzheimer's disease, Pharmacol. Ther. 116 (2007) 266–286.

[5] Y. Ling, K. Morgan, N. Kalsheker, Amyloid precursor protein (APP) and the biology of proteolytic processing: relevance to Alzheimer's disease, Int. J. Biochem. Cell Biol. 35 (2003) 1505–1535.

[6] M.d. Vestergaard, K. Kerman, E. Tamiya, The study of Alzheimer’s disease biomarkers, Nanobiotechnol. 2 (2006) 5–16.

[7] Y.K. Lee, K.-S. Lee, W.M. Kim, Y.-S. Sohn, Detection of amyloid-β42 using a waveguide-coupled bimetallic surface plasmon resonance sensor chip in the intensity measurement mode, PLoS ONE 9 (2014) e98992.

[8] J.P. Cleary, D.M. Walsh, J.J. Hofmeister, G.M. Shankar, M.A. Kuskowski, D.J. Selkoe, et al., Natural oligomers of the amyloid-beta protein specifically disrupt cognitive function, Nat. Neurosci. 8 (2005) 79–84.

[9] A. Afkhami, P. Hashemi, H. Bagheri, J. Salimian, A. Ahmadi, T. Madrakian, Impedimetric immunosensor for the label-free and direct detection of botulinum neurotoxin serotype A using Au nanoparticles/graphene-chitosan composite, Biosens. Bioelectron. 93 (2017) 124–131.

[10] R. Akter, B. Jeong, Y.-M. Lee, J.-S. Choi, M.A. Rahman, Femtomolar detection of cardiac troponin I using a novel label-free and reagent-free dendrimer enhanced impedimetric immunosensor, Biosens. Bioelectron. 91 (2017) 637–643.

[11] L.-G. Zamfir, I. Geana, S. Bourigua, L. Rotariu, C. Bala, A. Errachid, et al., Highly sensitive label-free immunosensor for ochratoxin A based on functionalized magnetic nanoparticles and EIS/SPR detection, Sens. Actuator B-Chem. 159 (2011) 178–184.

[12] T. Demeritte, B.P. Viraka Nellore, R. Kanchanapally, S.S. Sinha, A. Pramanik, S.R. Chavva, et al., Hybrid graphene oxide based plasmonic-magnetic multifunctional nanoplatform for selective separation and label-free identification of Alzheimer’s disease biomarkers, ACS Appl. Mater. Interfaces 7 (2015) 13693–13700.

[13] P. Gagni, L. Sola, M. Cretich, M. Chiari, Development of a high-sensitivity immunoassay for amyloid-beta 1–42 using a silicon microarray platform, Biosens. Bioelectron. 47 (2013) 490–495.

[14] M.K. Kang, J. Lee, A.H. Nguyen, S.J. Sim, Label-free detection of ApoE4-mediated β-amyloid aggregation on single nanoparticle uncovering Alzheimer's disease, Biosens. Bioelectron. 72 (2015) 197–204.

[15] M.-S. Chae, J. Kim, Y. Yoo, J. Lee, T. Kim, K. Hwang, Study of Alzheimer's disease-related biophysical kinetics with a microslit-embedded cantilever sensor in a liquid environment, Sensors 17 (2017) 1819.

[16] J.N. Anker, W.P. Hall, M.P. Lambert, P.T. Velasco, M. Mrksich, W.L. Klein, et al., Detection and identification of bioanalytes with high resolution LSPR spectroscopy and MALDI mass spectrometry, J Phys. Chem. C 113 (2009) 5891–5894.

[17] M.K. Mustafa, A. Nabok, D. Parkinson, I.E. Tothill, F. Salam, A. Tsargorodskaya, Detection of β-amyloid peptide (1–16) and amyloid precursor protein (APP_{770}) using spectroscopic ellipsometry and QCM techniques: A step forward towards Alzheimers disease diagnostics, Biosens. Bioelectron. 26 (2010) 1332–1336.

[18] M. Dragusanu, B.-A. Petre, S. Slamnoiu, C. Vlad, T. Tu, M. Przybylski, On-line bioaffinity-electrospray mass spectrometry for simultaneous detection, identification, and quantification of protein-ligand interactions, J. Am. Soc. Mass Spectrom. 21 (2010) 1643–1648.

[19] J.L. Hammond, N. Formisano, P. Estrela, S. Carrara, J. Tkac, Electrochemical biosensors and nanobiosensors, Essays Biochem. 60 (2016) 69-80.

[20] J. Park, H. Kim, J.-H. Lee, J. Park, J. Kim, K. Hwang, et al., Amyloid beta detection by faradaic electrochemical impedance spectroscopy using interdigitated microelectrodes, Sensors 18 (2018) 426.

[21] L. Han, P. Liu, V.A. Petrenko, A. Liu, A label-free electrochemical impedance cytosensor based on specific peptide-fused phage selected from landscape phage library, Sci. Rep. 6 (2016) 22199.

[22] E.P. Randviir, C.E. Banks, Electrochemical impedance spectroscopy: An overview of bioanalytical applications, Anal. Methods 5 (2013) 1098-1115.

[23] Z. Norazreen, M.Z. Zainiharyati, Development of impedimetric immunosensor for the detection of amyloid beta (1-40) on maβa/ortho-polyphenylenediamine modified platinum micro disk electrode, Int. J. Electrochem. Sci. 11 (2016) 872–881.

[24] L. Liu, B. Zhou, Electrochemical methods for detecting β-amyloid peptides and monitoring their aggregation, Int. J. Electrochem. Sci. 10 (2015) 7696–7706.

[25] J.V. Rushworth, A. Ahmed, H.H. Griffiths, N.M. Pollock, N.M. Hooper, P.A. Millner, A label-free electrical impedimetric biosensor for the specific detection of Alzheimer's amyloid-beta oligomers, Biosens. Bioelectron. 56 (2014) 83–90.

[26] D. Kim, A.E. Herr, Protein immobilization techniques for microfluidic assays, Biomicrofluidics 7 (2013) 41501.

[27] M.A. Rahman, M.J. Shiddiky, J.S. Park, Y.B. Shim, An impedimetric immunosensor for the label-free detection of bisphenol A, Biosens. Bioelectron. 22 (2007) 2464–2470.

[28] V. Mani, S.M. Jaafar, N.S.M. Azahan, K. Ramasamy, S.M. Lim, L.C. Ming, et al., Ciproxifan improves cholinergic transmission, attenuates neuroinflammation and oxidative stress but does not reduce amyloid level in transgenic mice, Life Sci. 180 (2017) 23–35.

[29] V.F. Lvovich, Impedance Spectroscopy: Applications to Electrochemical and Dielectric Phenomena, reprint ed., Wiley, New Jersey, 2015.

[30] M.E. Orazem, B. Tribollet, Electrochemical Impedance Spectroscopy, second ed., Wiley: New Jersey, 2017.

[31] B. Viguier, K. Zór, E. Kasotakis, A. Mitraki, C.H. Clausen, W.E. Svendsen, et al., Development of an electrochemical metal-ion biosensor using self-assembled peptide nanofibrils, ACS Appl. Mater. Interfaces 3 (2011) 1594–1600.

[32] L. Truong TN, V. Nguyen Xuan, M. Chikae, Y. Ukita, Y. Takamura, Development of label-free impedimetric hCG-immunosensor using screen-printed electrode, J. Biosens. Bioelectron. 2 (2011) 107.

[33] R.K. Shervedani, A.H. Mehrjardi, N. Zamiri, A novel method for glucose determination based on electrochemical impedance spectroscopy using glucose oxidase self-assembled biosensor, Bioelectrochemistry 69 (2006) 201–208.

[34] F. Malvano, L. Maritato, G. Carapella, P. Orgiani, R. Pilloton, M. Di Matteo, et al., Fabrication of $SrTiO_3$ layer on Pt electrode for label-free capacitive biosensors, Biosensors 8 (2018) 26.

[35] H.A. Lashuel, D.M. Hartley, B.M. Petre, J.S. Wall, M.N. Simon, T. Walz, et al., Mixtures of wild-type and a pathogenic (E22G) form of Abeta40 *in vitro* accumulate protofibrils, including amyloid pores, J. Mol. Biol. 332 (2003) 795–808.

[36] S.-S. Li, C.-W. Lin, K.-C. Wei, C.-Y. Huang, P.-H. Hsu, H.-L. Liu, et al., Non-invasive screening for early Alzheimer's disease diagnosis by a sensitively immunomagnetic biosensor, Sci. Rep. 6 (2016) 25155.

[37] P. Carneiro, J. Loureiro, C. Delerue-Matos, S. Morais, M. do Carmo Pereira, Alzheimer's disease: Development of a sensitive label-free electrochemical immunosensor for detection of amyloid beta peptide, Sens. Actuator B-Chem. 239 (2017) 157–165.

[38] A. Kaushik, P. Shah, P.K. Vabbina, R.D. Jayant, S. Tiwari, A. Vashist, et al., A label-free electrochemical immunosensor for beta-amyloid detection, Anal. Methods 8 (2016) 6115–6120.

[39] T.T.N. Lien, Y. Takamura, E. Tamiya, M.d.C. Vestergaard, Modified screen printed electrode for development of a highly sensitive label-free impedimetric immunosensor to detect amyloid beta peptides, Anal. Chim. Acta 892 (2015) 69–76.

[40] S. Prabhulkar, R. Piatyszek, J.R. Cirrito, Z.Z. Wu, C.Z. Li, Microbiosensor for Alzheimer's disease diagnostics: detection of amyloid beta biomarkers, J. Neurochem. 122 (2012) 374–381.

[41] S. Kirwan, G. Rocchitta, C. McMahon, J. Craig, S. Killoran, K. O'Brien, et al., Modifications of poly(o-phenylenediamine) permselective payer on Pt-Ir for biosensor application in neurochemical monitoring, Sensors 7 (2007) 420–437.

[42] D. Puzzo, L. Privitera, M. Fa, A. Staniszewski, G. Hashimoto, F. Aziz, et al., Endogenous amyloid-β is necessary for hippocampal synaptic plasticity and memory, Ann. Neurol. 69 (2011) 819–830.

[43] N.T. Thuy, T.T. Tseng, A micro-platinum wire biosensor for fast and selective detection of alanine aminotransferase, Sensors 16 (6) 767.

[44] J. Rodrigo, P. Fernandez-Vizarra, S. Castro-Blanco, M.L. Bentura, M. Nieto, T. Gomez-Isla, et al., Nitric oxide in the cerebral cortex of amyloid-precursor protein (SW) Tg2576 transgenic mice, Neurosci. 128 (2004) 73–89.

[45] F.S. Diba, S. Kim, H.J. Lee, Electrochemical immunoassay for amyloid-beta 1–42 peptide in biological fluids interfacing with a gold nanoparticle modified carbon surface, Catal. Today 295 (2017) 41–47.

Table caption

Table 1. Grouping of animals and experimental treatment.

Table 2. Comparison of the developed impedimetric micro-immunosensing assay with the reported label-free electrochemical immunosensing platforms for Aβ detection.

Figure captions

Fig. 1. A schematic of the micro-immunosensing assay for impedimetric label-free detection of Aβ40. The experimental procedures comprised: (1) Electropolymerization of PoPD on a Pt/Ir microelectrode surface; (2) Covalent immobilization of *m*$A\beta_{ab}$ on a PoPD-modified Pt/Ir microelectrode surface via GA crosslinking; (3) Immuno-capturing of Aβ40; and (4) Quantitative electrochemical detection of target Aβ40 using an impedance technique.

Fig. 2. Equivalent circuit model of the micro-immunosensing assay.

Fig. 3. Schematic representation of the reaction mechanisms occurring during the preparation of the *m*$A\beta_{ab}$–GA–PoPD-modified Pt/Ir microelectrode and subsequent detection of Aβ40.

Fig. 4. (A) FESEM images of (i) bare, (ii) PoPD-modified, (iii) *m*$A\beta_{ab}$–GA–PoPD-modified, and (iv) Aβ40–*m*$A\beta_{ab}$–GA–PoPD-modified Pt/Ir microelectrodes under 10, 000 × magnification. (B) Nyquist plots of PoPD-modified (x-line), GA–PoPD-modified (□-line), *m*$A\beta_{ab}$–GA–PoPD-modified (Δ-line), and Aβ40–*m*$A\beta_{ab}$–GA–PoPD-modified (◊-line) Pt/Ir microelectrodes. Inset: Nyquist plot of a representative bare Pt/Ir microelectrode.

Fig. 5. (A) Analytical sensitivity evaluation of the impedimetric micro-immunosensing assay using a known amount of serially diluted Aβ40. The corresponding linear range is depicted in the calibration plot. (B) Analytical specificity evaluation of the impedimetric micro-immunosensing assay using different interference species. The error bars indicate the standard deviation from triplicate experiments (n = 3).

Fig. 6. Comparison of the impedimetric micro-immunosensing assay and ELISA for detecting Aβ40 in rat brain tissue lysate samples. The error bars show the standard deviation from triplicate experiments (n = 3).

LIST OF TABLE

Table 1. Grouping of animals and experimental treatment.

Group (n = 4)	Experimental treatment
Wild Type (WT)	Normal rats serving as the negative control group.
Sham (SH)	Sham-operated rats given no injection into the brain.
AD	Animal models mimicking AD, which was induced by injection of synthetic Aβ into the brain.
AD + olive oil (AD+O)	AD-induced rats treated with olive oil and serving as the therapeutic positive control group.
AD +ibuprofen (AD+IB)	AD-induced rats treated with ibuprofen and serving as the therapeutic positive control group.

Table 2. Comparison of the developed impedimetric micro-immunosensing assay with the reported label-free electrochemical immunosensing platforms for Aβ detection.

Electrode	Immobilization of capturing antibody	Electroanalytical technique	LoD (pg/mL)	Liner range (pg/mL)	Ref.
Disc-shaped Pt/Ir microelectrode	Covalent coupling; Ab–GA–PoPD	EIS	4.81	$1–10^4$ $R^2 = 0.9932$	This study
Screen-printed gold electrode	Covalent coupling; Ab–sulfo-SMCC–MNG	DPV	5	5–800 $R^2 = 0.9977$	[36]
Gold electrode	Dative binding; Ab–GNP−MPA	SWV	5.2	$10–10^3$ $R^2 = 0.9643$	[37]
Gold interdigitated electrode	Covalent coupling Ab–DTSP	EIS	43.3***	43.3***–4.33×10^5 $R^2 = 0.99$	[38]
Carbon disposable electrochemical printed chip	Non-covalent binding; Ab–Protein G–EDC/NHS–MHDA–GNP	EIS	2.57×10^3**	45.14***–4.51×10^5** $R^2 = 0.9969$	[39]
Carbon fiber microelectrode	Covalent binding; Ab–EDC/NHS–carboxylic functionalities on electrode surface	SWV	9.03×10^4**	9.03×10^4**–6.32×10^5** R^2 = Not provided	[40]
Disc-shaped Pt/Ir microelectrode	Passive adsorption; Ab–PoPD	EIS	1.08×10^6*	1.08×10^6*–4.22×10^7* R^2 = 0.9622	[23]

* Value was expressed in μM and converted to pg/mL
** Value was expressed in nM and converted to pg/mL
*** Value was expressed in pM and converted to pg/mL

Abbreviations: Ab (antibody); GA (glutaraldehyde); PoPD (poly(ortho-phenylenediamine)); MPA (mercaptopropionic acid); GNP (gold nanoparticle); EDC (1-Ethyl-3-(3-dimethylaminopropyl) Carbodiimide); NHS (N-hydroxysuccinimide); MHDA (16-mercaptohexadecanoic acid); sulfo-SMCC (sulfosuccinimidyl-4-(N-maleimidomethyl)cyclohexane-1-carboxylate); MNG (magnetic nitrogen-doped graphene); DTSP (dithiobis(succinimidyl propionate));

List of Figures

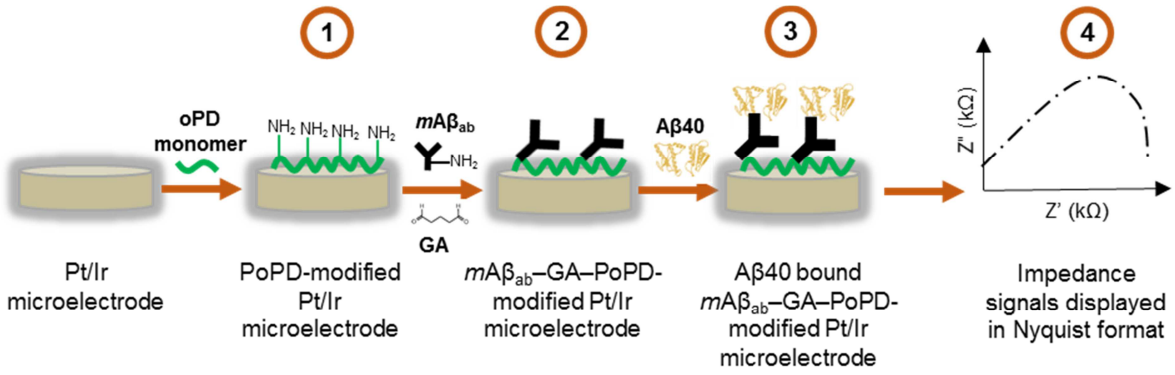

Fig. 1. A schematic of the micro-immunosensing assay for impedimetric label-free detection of Aβ40. The experimental procedures comprised: (1) Electropolymerization of PoPD on a Pt/Ir microelectrode surface; (2) Covalent immobilization of $m\text{A}\beta_{ab}$ on a PoPD-modified Pt/Ir microelectrode surface via GA crosslinking; (3) Immuno-capturing of Aβ40; and (4) Quantitative electrochemical detection of target Aβ40 using an impedance technique.

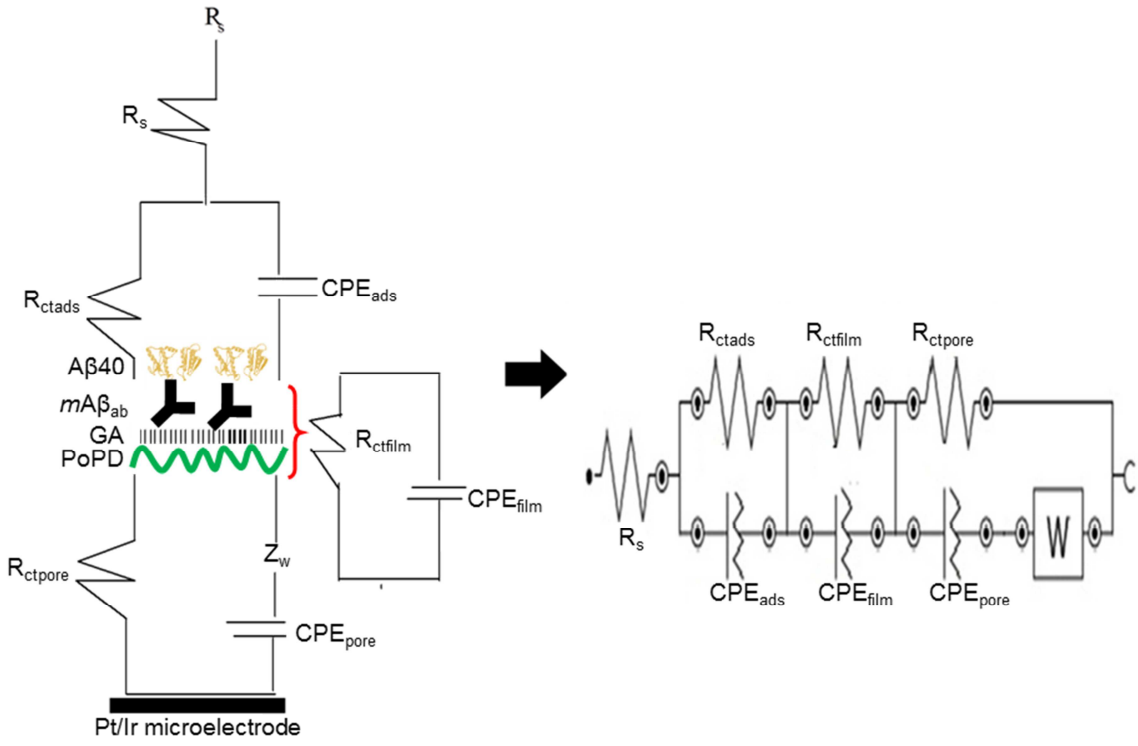

Fig. 2. Equivalent circuit model of the micro-immunosensing assay.

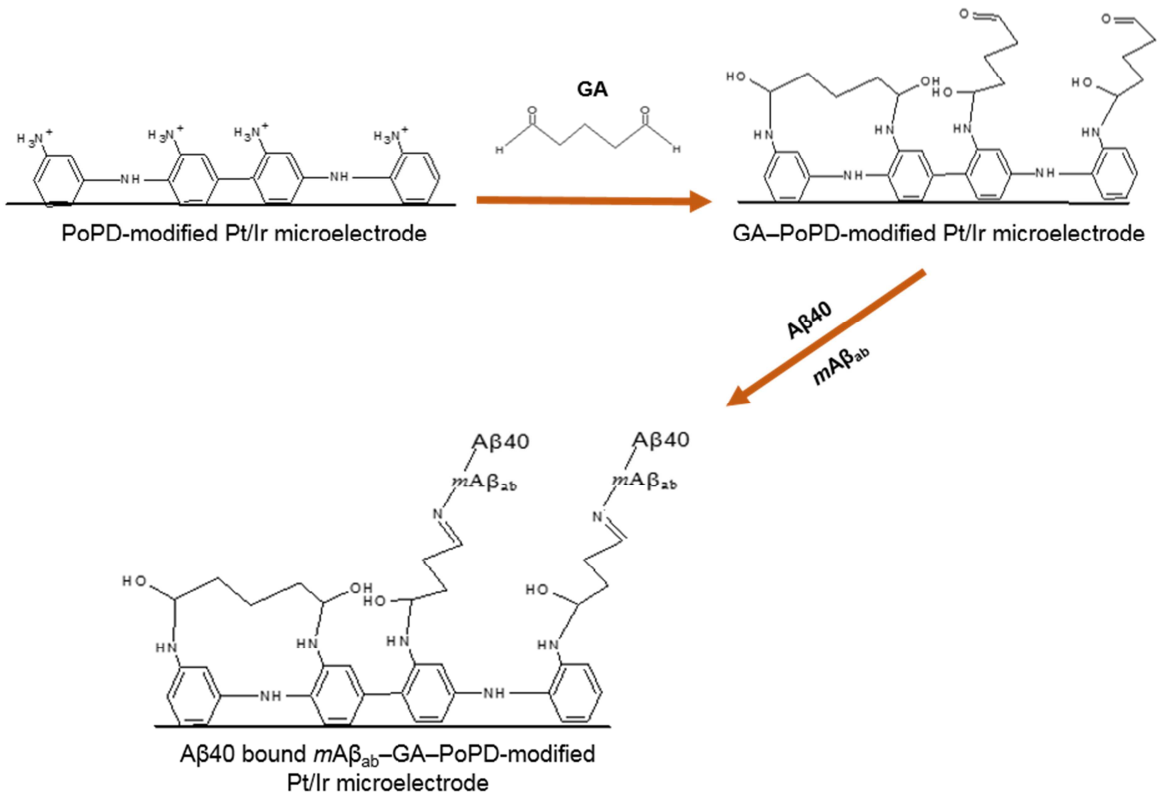

Fig. 3. Schematic representation of the reaction mechanisms occurring during the preparation of the *m*Aβ$_{ab}$–GA–PoPD-modified Pt/Ir microelectrode and subsequent detection of Aβ40.

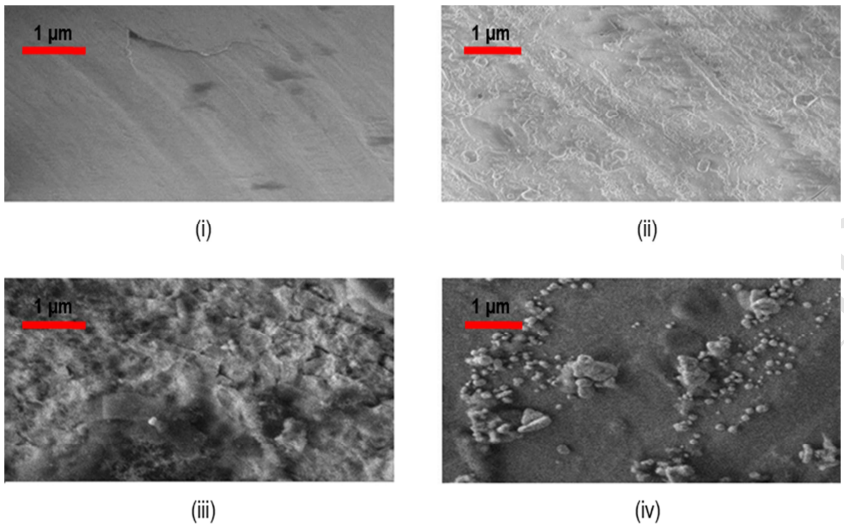

(A)

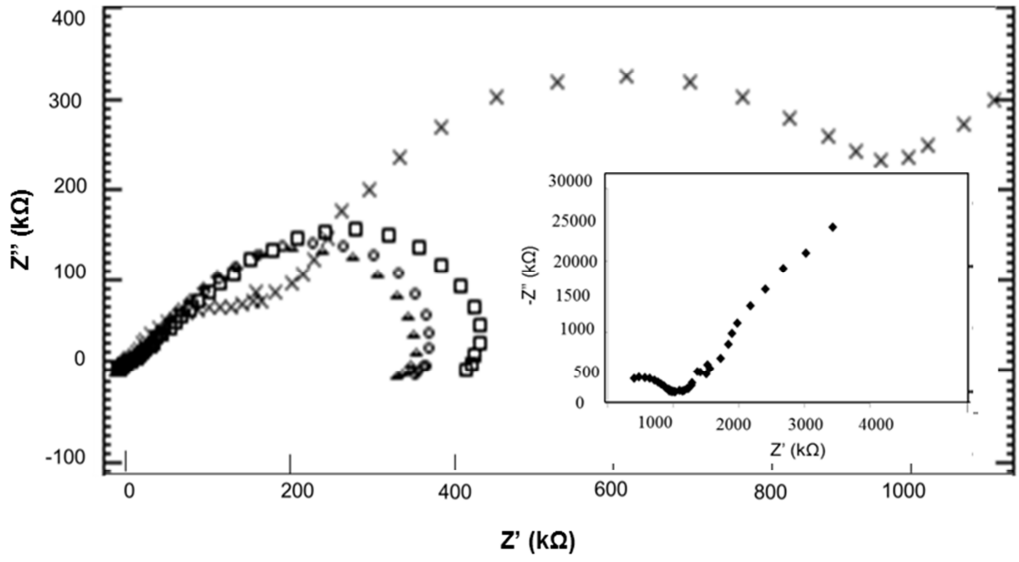

(B)

Fig. 4. (A) FESEM images of (i) bare, (ii) PoPD-modified, (iii) *m*Aβ$_{ab}$–GA–PoPD-modified, and (iv) Aβ40–*m*Aβ$_{ab}$–GA–PoPD-modified Pt/Ir microelectrodes under 10, 000 × magnification. (B) Nyquist plots of PoPD-modified (x-line), GA–PoPD-modified (□-line), *m*Aβ$_{ab}$–GA–PoPD-modified (Δ-line), and Aβ40–*m*Aβ$_{ab}$–GA–PoPD-modified (◊-line) Pt/Ir microelectrodes. Inset: Nyquist plot of a representative bare Pt/Ir microelectrode.

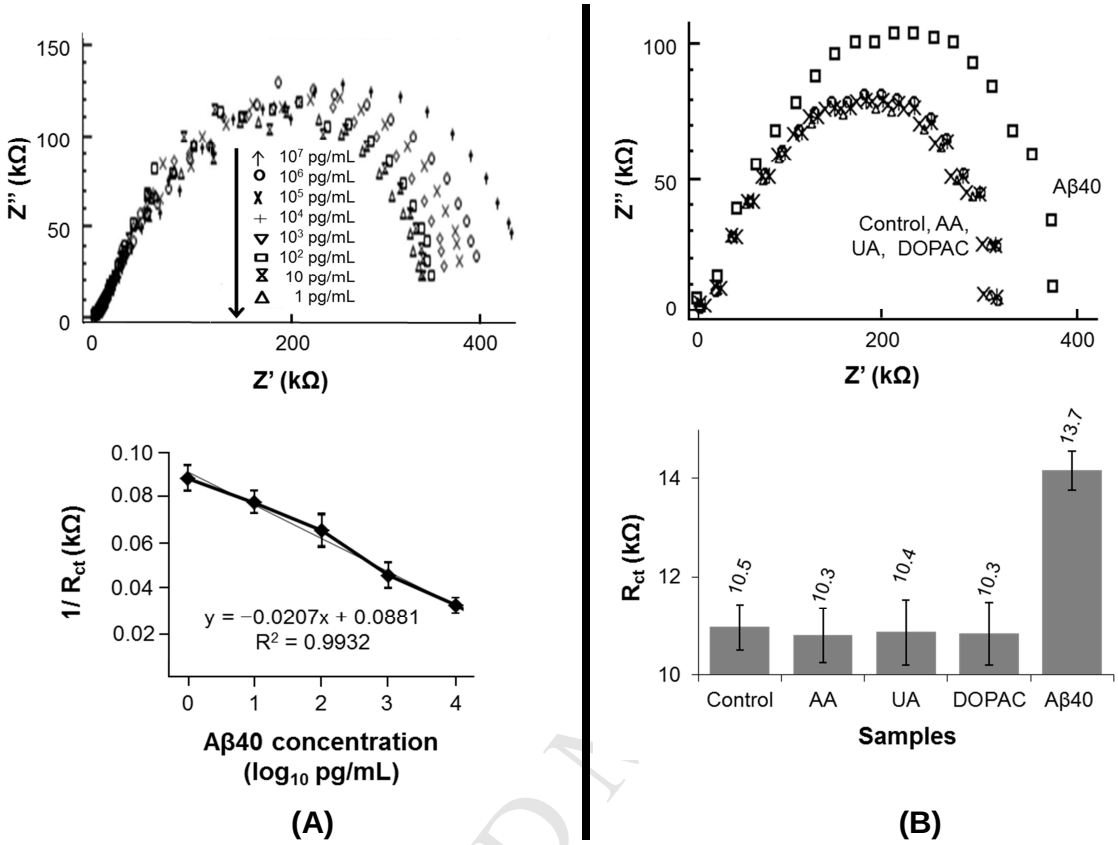

Fig. 5. (A) Analytical sensitivity evaluation of the impedimetric micro-immunosensing assay using a known amount of serially diluted Aβ40. The corresponding linear range is depicted in the calibration plot. (B) Analytical specificity evaluation of the impedimetric micro-immunosensing assay using different interference species. The error bars indicate the standard deviation from triplicate experiments (n = 3).

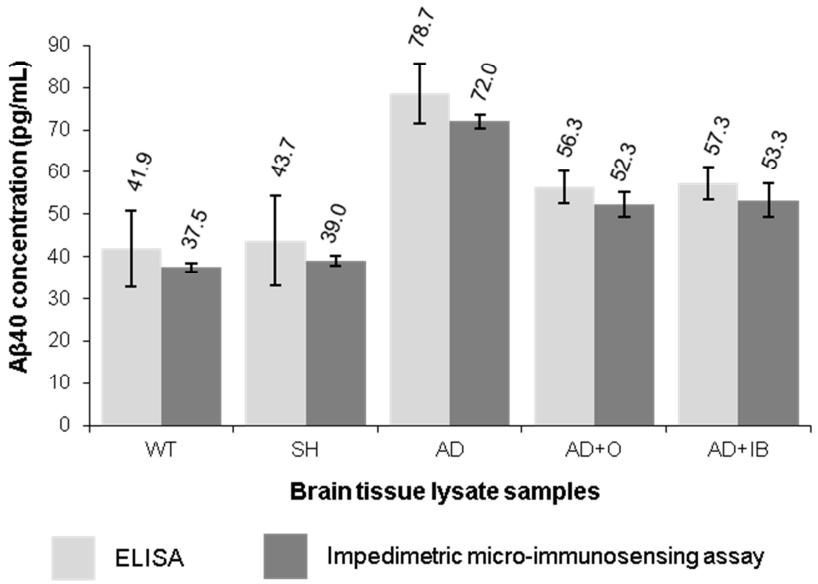

Fig. 6. Comparison of the impedimetric micro-immunosensing assay and ELISA for detecting Aβ40 in rat brain tissue lysate samples. The error bars show the standard deviation from triplicate experiments (n = 3).

Highlights

- A novel impedimetric micro-immunosensing assay for Alzheimer's disease (AD) biomarker detection was developed.
- A glutaraldehyde crosslinking-covalent coupling strategy was employed to immobilize biorecognition antibodies on a microelectrode surface.
- Immuno-interactions were determined by detecting impedance changes in terms of charge transfer resistance at the electrode–electrolyte interface.
- This impedimetric micro-immunosensing assay was able to detect the AD biomarker, Aβ40, in brain tissue lysate.